Appl. Math. Mech. -Engl. Ed., **39**(11), 1587–1604 (2018)

Applied Mathematics and Mechanics (English Edition)

https://doi.org/10.1007/s10483-018-2388-6

Identifying the temperature effect on the vibrations of functionally graded cylindrical shells with porosities*

Yanqing WANG[1,2,†], Chao YE[1], J. W. ZU[3]

1. Department of Mechanics, Northeastern University, Shenyang 110819, China;
2. Key Laboratory of Ministry of Education on Safe Mining of Deep Metal Mines, Northeastern University, Shenyang 110819, China;
3. Schaefer School of Engineering and Science, Stevens Institute of Technology, Hoboken, NJ 07030, U. S. A.

(Received Mar. 2, 2018 / Revised Jun. 7, 2018)

Abstract The free thermal vibration of functionally graded material (FGM) cylindrical shells containing porosities is investigated. Both even distribution and uneven distribution are taken into account. In addition, three thermal load types, i.e., uniform temperature rise (UTR), nonlinear temperature rise (NLTR), and linear temperature rise (LTR), are researched to explore their effects on the vibration characteristics of porous FGM cylindrical shells. A modified power-law formulation is used to describe the material properties of FGM shells in the thickness direction. Love's shell theory is used to formulate the strain-displacement equations, and the Rayleigh-Ritz method is utilized to calculate the natural frequencies of the system. The results show that the natural frequencies are affected by the porosity volume fraction, constituent volume fraction, and thermal load. Moreover, the natural frequencies obtained from the LTR have insignificant differences compared with those from the NLTR. Due to the calculation complexity of the NLTR, we propose that it is reasonable to replace it by its linear counterpart for the analysis of thin porous FGM cylindrical shells. The present results are verified in comparison with the published ones in the literature.

Key words functionally graded material (FGM), cylindrical shell, porosity, free vibration, thermal load, Rayleigh-Ritz method

Chinese Library Classification O321
2010 Mathematics Subject Classification 74H45

1 Introduction

The concept of functionally graded materials (FGMs) was first presented by a group of scientists in Japan[1]. As a new type of composite materials, FGMs usually consist of two

* Citation: WANG, Y. Q., YE, C., and ZU, J. W. Identifying the temperature effect on the vibrations of functionally graded cylindrical shells with porosities. *Applied Mathematics and Mechanics* (*English Edition*), **39**(11), 1587–1604 (2018) https://doi.org/10.1007/s10483-018-2388-6

† Corresponding author, E-mail: wangyanqing@mail.neu.edu.cn

Project supported by the National Natural Science Foundation of China (No. 11672071) and the Fundamental Research Funds for the Central Universities (No. N170504023)

or more materials[2–7]. Their component volume fraction changes continuously in the spatial field, resulting in a graded variation in the material properties. Such design can impart the properties of the components to the combinations, e.g., the FGMs composed of metals and heat-resistant materials have the advantages of both the materials. Moreover, FGMs possess heat resistance at one surface, and have good ductility at the other one, which makes them easy to be processed. Nowadays, FGMs have shown remarkable performances in the fields such as aerospace, mechanical engineering, and national defense, and have exhibited great development prospects.

FGM circular cylindrical shells are common FGM structures in real applications. For a material, the dynamics analysis is of importance for its structural design and applications[8]. Therefore, the vibrations of FGM shells have been widely studied. Loy et al.[9] carried out a vibration analysis on an FGM cylindrical shell made of stainless steel and nickel for the first time, and used the Rayleigh-Ritz method to solve the natural frequencies of the simply supported shell. Patel et al.[10] analyzed the free vibration of FGM elliptical cylindrical shells via the high-order theory. Shah et al.[11] studied the effects of an exponential volume fraction law on the vibration frequencies of thin FGM cylindrical shells. Based on the two-dimensional (2D) high-order deformation theory, Matsunaga[12] solved the vibration and buckling problems of circular cylindrical shells made of FGMs. Arshad et al.[13] presented the vibration frequency analysis of a bi-layered cylindrical shell composed of two independent FGM layers. Ding et al.[14] and Tan et al.[15] contributed to solving the natural frequency of a structure after it was buckled due to high-speed movement and flow, respectively. They took the lead in discovering that the natural frequency did not change monotonically with the bending stiffness. Carrera et al.[16] studied the effect of thickness stretching on FGM plates and shells. Bich and Xuan[17] investigated the nonlinear vibration of an FGM cylindrical shell subject to axial and transverse mechanical loads. Strozzi and Pellicano[18] dealt with the nonlinear vibrations of FGM cylindrical shells, and modeled the system with the Sanders-Koiter theory. Tornabene et al.[19] conducted the dynamic analysis of doubly-curved shell structures based on the generalized displacement field of the Carrera unified formulation.

FGM structures usually work in thermal environment. Therefore, understanding the thermal vibration characteristics of FGM cylindrical shells is very important. Considering the thermal effect, Bhangle et al.[20] studied the linear free vibration of FGM truncated conical shells. Haddadpour et al.[21] investigated the free vibration of FGM cylindrical shells incorporating the thermal effects. Zhao et al.[22] analyzed the thermoelastic response and free vibration of metal-ceramic FGM cylindrical shells. Kiani et al.[23] analyzed the FGM doubly curved panels with rectangular planform under the action of thermal and mechanical loads. Zhang et al.[24] studied the nonlinear forced vibration of thin FGM cylindrical shells subject to linear temperature change. Du et al.[25] investigated the nonlinear vibrations of FGM cylindrical thin shells in thermal environment. Liu et al.[26] studied the nonlinear thermal vibration of a simply supported FGM cylindrical shell with small initial geometric imperfection under complex loads. Using Reddy's third-order shear deformation shell theory, Duc[27] presented an investigation on the nonlinear thermal dynamic behavior of imperfect FGM circular cylindrical shells eccentrically reinforced by outside stiffeners and surrounded on elastic foundations. Considering the linear temperature field, Sheng and Wang[28] studied the nonlinear vibrations of rotating FGM cylindrical shells.

Due to the limitation of FGM manufacture technology, the porosities can possibly occur in the manufacturing process[29]. Wattanasakulpong and Chaikittiratana[30] studied the vibrations of FGM beams with porosities, and obtained the natural frequencies with the Chebyshev collocation method. Ebrahimi et al.[31] investigated the vibration of compositionally graded Euler beams with porosities, and showed that several parameters such as the thermal effect and the porosity volume fraction had a significant effect on the natural frequencies. Recently, Wang and Zu[32] and Wang[33] analyzed the nonlinear vibration of FGM plates with porosities,

and found that porosities had a significant effect on the vibration characteristics of the FGM plates.

Though porosities can affect the dynamics behavior of FGM structures, the vibration analysis on FGM cylindrical shells with porosities has still not been reported. Especially, the effect of various temperature types on this imperfect structure needs to be clarified. In this paper, we aim to identify the difference of various temperature types on the vibration characteristic of FGM cylindrical shells with porosities. Three thermal load types, i.e., uniform temperature rise (UTR), nonlinear temperature rise (NLTR), and linear temperature rise (LTR), are considered. Two porosity distributions, i.e., even distribution and uneven distribution, are taken into account. The geometric mathematical model is deduced by Love's shell theory, and the solutions are obtained with the Rayleigh-Ritz method. In addition, the effects of some key system parameters are investigated on the vibrations of the FGM shells with porosities.

2 FGM cylindrical shells with porosities

We consider a porous FGM cylindrical shell composed of ceramic (Al_2O_3) and nickel. The inner surface is pure nickel, which changes continually to ceramic at the outer surface. The porosities inside the shell disperse evenly or unevenly along the thickness direction (see Fig. 1). The geometry of the shell is defined by the middle-surface radius R, the thickness h, and the length L. A coordinate system (x, θ, z) is chosen at the middle surface of the shell. The displacement components of points at the mid-plane of the shell are denoted by $u(x,\theta,t)$, $v(x,\theta,t)$, and $w(x,\theta,t)$ in the x-, θ-, and z-directions from the static equilibrium ($u = v = w = 0$), respectively.

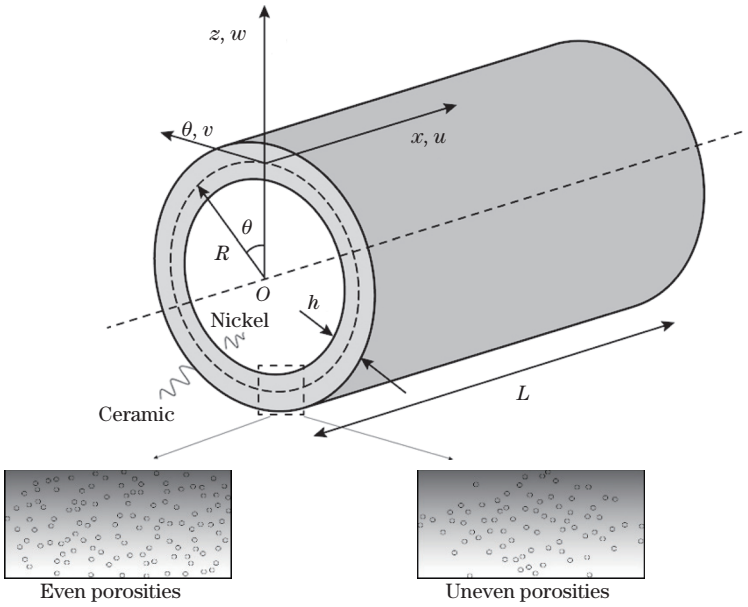

Fig. 1 An FGM cylindrical shell with porosities

The temperature-dependent properties of constituent materials can be written as follows[9]:

$$P = P_0(P_{-1}T^{-1} + 1 + P_1T + P_2T^2 + P_3T^3), \tag{1}$$

where P_0, P_{-1}, P_1, P_2, and P_3 are the temperature coefficients of the constituent materials, and T is the Kelvin temperature.

When the porosities disperse equally in the nickel and ceramic phases, the effective material property of the FGM shell takes the modified form as follows:

$$P(z,T)=P_{\mathrm{M}}(T)\Big(V_{\mathrm{M}}(z)-\frac{\alpha}{2}\Big)+P_{\mathrm{C}}(T)\Big(V_{\mathrm{C}}(z)-\frac{\alpha}{2}\Big), \tag{2}$$

where α ($\alpha \ll 1$) is the porosity volume fraction. P_{M} and P_{C} are the material properties of metal and ceramic, respectively. V_{M} and V_{C} are the volume fractions of metal and ceramic, respectively.

The sum of both the volume fractions should be $V_{\mathrm{M}}(z)+V_{\mathrm{C}}(z)=1$[30]. The volume fraction of the FGM shell is supposed to change continually across the thickness direction and obey the power-law distribution as follows[34]:

$$V_{\mathrm{C}}(z)=\Big(\frac{z}{h}+\frac{1}{2}\Big)^{N}, \tag{3}$$

where $N\in[0,\infty)$ is the power-law index.

For the FGM shell with evenly distributed porosities (Porosity-I for short), the general Poisson's ratio μ, the elastic modulus E, the mass density ρ, the thermal conductivity κ, and the thermal expansion coefficient α_{T} can be expressed as follows:

$$\mu(z,T)=(\mu_{\mathrm{C}}(T)-\mu_{\mathrm{M}}(T))\Big(\frac{z}{h}+\frac{1}{2}\Big)^{N}+\mu_{\mathrm{M}}(T)-\frac{\alpha}{2}(\mu_{\mathrm{C}}(T)+\mu_{\mathrm{M}}(T)), \tag{4}$$

$$E(z,T)=(E_{\mathrm{C}}(T)-E_{\mathrm{M}}(T))\Big(\frac{z}{h}+\frac{1}{2}\Big)^{N}+E_{\mathrm{M}}(T)-\frac{\alpha}{2}(E_{\mathrm{C}}(T)+E_{\mathrm{M}}(T)), \tag{5}$$

$$\rho(z,T)=(\rho_{\mathrm{C}}(T)-\rho_{\mathrm{M}}(T))\Big(\frac{z}{h}+\frac{1}{2}\Big)^{N}+\rho_{\mathrm{M}}(T)-\frac{\alpha}{2}(\rho_{\mathrm{C}}(T)+\rho_{\mathrm{M}}(T)), \tag{6}$$

$$\kappa(z)=(\kappa_{\mathrm{C}}-\kappa_{\mathrm{M}})\Big(\frac{z}{h}+\frac{1}{2}\Big)^{N}+\kappa_{\mathrm{M}}-\frac{\alpha}{2}(\kappa_{\mathrm{C}}+\kappa_{\mathrm{M}}), \tag{7}$$

$$\alpha_{\mathrm{T}}(z,T)=(\alpha_{\mathrm{T,C}}(T)-\alpha_{\mathrm{T,M}}(T))\Big(\frac{z}{h}+\frac{1}{2}\Big)^{N}+\alpha_{\mathrm{T,M}}(T)-\frac{\alpha}{2}(\alpha_{\mathrm{T,C}}(T)+\alpha_{\mathrm{T,M}}(T)), \tag{8}$$

where the thermal conductivity is assumed to be temperature independent due to its small change with temperature.

For the FGM shell with unevenly distributed porosities (Porosity-II for short), the general material properties in Eqs. (4), (5), (6), (7), and (8) can be replaced by[30]

$$\mu(z,T)=(\mu_{\mathrm{C}}(T)-\mu_{\mathrm{M}}(T))\Big(\frac{z}{h}+\frac{1}{2}\Big)^{N}+\mu_{\mathrm{M}}(T)-\frac{\alpha}{2}(\mu_{\mathrm{C}}(T)+\mu_{\mathrm{M}}(T))\Big(1-\frac{2|z|}{h}\Big), \tag{9}$$

$$E(z,T)=(E_{\mathrm{C}}(T)-E_{\mathrm{M}}(T))\Big(\frac{z}{h}+\frac{1}{2}\Big)^{N}+E_{\mathrm{M}}(T)-\frac{\alpha}{2}(E_{\mathrm{C}}(T)+E_{\mathrm{M}}(T))\Big(1-\frac{2|z|}{h}\Big), \tag{10}$$

$$\rho(z,T)=(\rho_{\mathrm{C}}(T)-\rho_{\mathrm{M}}(T))\Big(\frac{z}{h}+\frac{1}{2}\Big)^{N}+\rho_{\mathrm{M}}(T)-\frac{\alpha}{2}(\rho_{\mathrm{C}}(T)+\rho_{\mathrm{M}}(T))\Big(1-\frac{2|z|}{h}\Big), \tag{11}$$

$$\kappa(z)=(\kappa_{\mathrm{C}}-\kappa_{\mathrm{M}})\Big(\frac{z}{h}+\frac{1}{2}\Big)^{N}+\kappa_{\mathrm{M}}-\frac{\alpha}{2}(\kappa_{\mathrm{C}}+\kappa_{\mathrm{M}})\Big(1-\frac{2|z|}{h}\Big), \tag{12}$$

$$\begin{aligned}\alpha_{\mathrm{T}}(z,T)=&(\alpha_{\mathrm{T,C}}(T)-\alpha_{\mathrm{T,M}}(T))\Big(\frac{z}{h}+\frac{1}{2}\Big)^{N}+\alpha_{\mathrm{T,M}}(T)\\&-\frac{\alpha}{2}(\alpha_{\mathrm{T,C}}(T)+\alpha_{\mathrm{T,M}}(T))\Big(1-\frac{2|z|}{h}\Big).\end{aligned} \tag{13}$$

3 Various thermal load types

3.1 UTR

A circular cylindrical porous FGM shell at the initial reference temperature T_0 is assumed. Under the UTR condition, the temperature of the whole shell is uniformly raised to a final value T, which can be expressed as follows:

$$T = T_0 + \Delta T_0, \tag{14}$$

where ΔT_0 stands for the temperature difference between the initial temperature and the final temperature of the shell.

3.2 NLTR

Assume that the porous FGM cylindrical shell is in the temperature field, where the temperature varies only along the thickness direction. Then, we have that the temperature distribution should satisfy the one-dimensional (1D) steady-state heat transfer equation in the case of no heat source, i.e.,

$$-\frac{\mathrm{d}}{\mathrm{d}z}\Big(\kappa(z)\frac{\mathrm{d}T}{\mathrm{d}z}\Big) = 0 \tag{15}$$

with the boundary condition

$$T = \begin{cases} T_{\mathrm{M}}, & z = -\dfrac{h}{2}, \\ T_{\mathrm{C}}, & z = \dfrac{h}{2}. \end{cases} \tag{16}$$

Solving Eqs. (15) and (16), we can obtain the solution T, which is a nonlinear function of z and the porosity volume fraction α. This expression has a quite complex form. Thus, we express T as follows:

$$T(z) = F_{\mathrm{NL}}(z, \alpha, T_{\mathrm{M}}, \Delta T_1, \kappa_{\mathrm{C}}, \kappa_{\mathrm{M}}), \tag{17}$$

where $\Delta T_1 = T_{\mathrm{C}} - T_{\mathrm{M}}$.

Note that Javaheri and Eslami[35] have also solved Eqs. (15) and (16) in the condition without porosities. In their study, the temperature function T is only related to z, i.e.,

$$\begin{aligned} T(z) = {} & T_{\mathrm{M}} + \frac{\Delta T_1}{C}\Big(\Big(\frac{z}{h}+\frac{1}{2}\Big) - \frac{\kappa_{\mathrm{CM}}}{(N+1)\kappa_{\mathrm{M}}}\Big(\frac{z}{h}+\frac{1}{2}\Big)^{N+1} + \frac{\kappa_{\mathrm{CM}}^2}{(2N+1)\kappa_{\mathrm{M}}^2}\Big(\frac{z}{h}+\frac{1}{2}\Big)^{2N+1} \\ & - \frac{\kappa_{\mathrm{CM}}^3}{(3N+1)\kappa_{\mathrm{M}}^3}\Big(\frac{z}{h}+\frac{1}{2}\Big)^{3N+1} + \frac{\kappa_{\mathrm{CM}}^4}{(4N+1)\kappa_{\mathrm{M}}^4}\Big(\frac{z}{h}+\frac{1}{2}\Big)^{4N+1} \\ & - \frac{\kappa_{\mathrm{CM}}^5}{(5N+1)\kappa_{\mathrm{M}}^5}\Big(\frac{z}{h}+\frac{1}{2}\Big)^{5N+1}\Big) \end{aligned} \tag{18}$$

with

$$C = 1 - \frac{\kappa_{\mathrm{CM}}}{(N+1)\kappa_{\mathrm{M}}} + \frac{\kappa_{\mathrm{CM}}^2}{(2N+1)\kappa_{\mathrm{M}}^2} - \frac{\kappa_{\mathrm{CM}}^3}{(3N+1)\kappa_{\mathrm{M}}^3} + \frac{\kappa_{\mathrm{CM}}^4}{(4N+1)\kappa_{\mathrm{M}}^4} - \frac{\kappa_{CM}^5}{(5N+1)\kappa_{\mathrm{M}}^5}, \tag{19}$$

$$\kappa_{\mathrm{CM}} = \kappa_{\mathrm{C}} - \kappa_{\mathrm{M}}. \tag{20}$$

To compare the present results with those not including the porosity effect, we plot Fig. 2. When we set $\alpha = 0$ (without porosity), the present temperature curve coincides with that given by Javaheri and Eslami[35] (see Fig. 2(a)). When we set the porosity volume fraction as $\alpha = 0.2$, a small difference between these two results can be detected (see Figs. 2(b) and 2(c)). This demonstrates that porosities have a very limited effect on the temperature distribution.

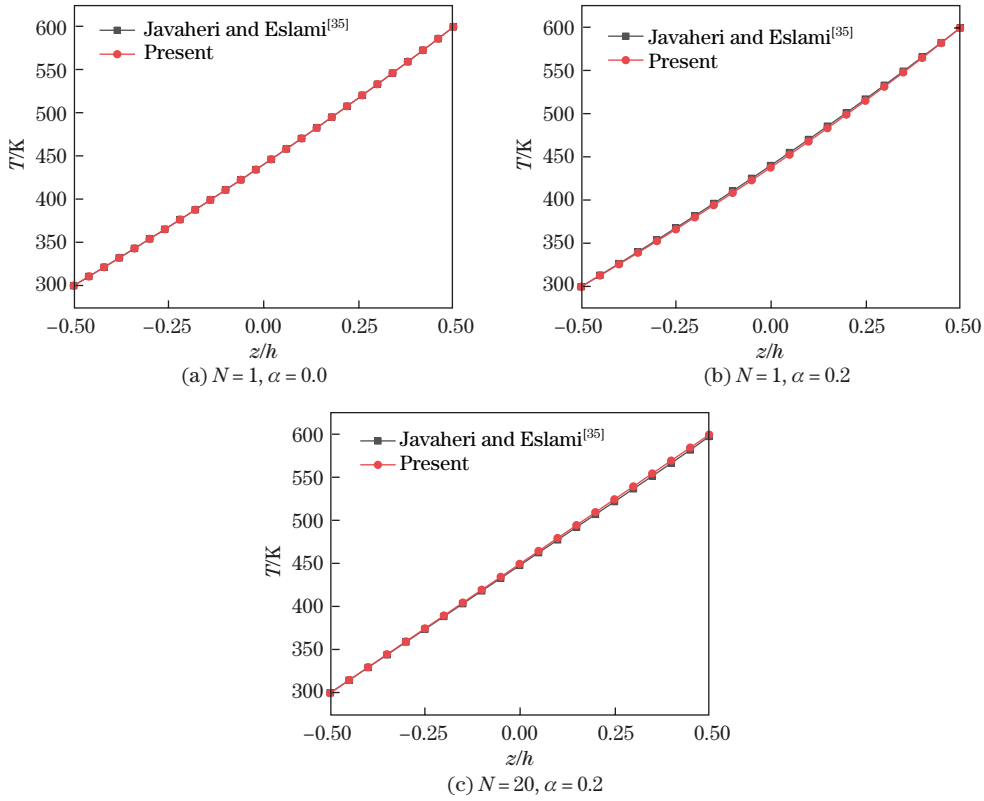

Fig. 2 Comparison of the nonlinear temperature functions with and without porosities (color online)

3.3 LTR

Due to the limited effect of porosities, the temperature distribution of Eq. (17) can be approximated by the linear temperature change as follows[35]:

$$T(z) = T_{\mathrm{M}} + \Delta T_1 \left(\frac{z}{h} + \frac{1}{2} \right), \tag{21}$$

which means that the temperature function T linearly increases with z.

4 Governing equations and solution procedure

Under the plane stress condition, the stress-strain relation of a thin FGM cylindrical shell can be expressed as follows[36]:

$$\begin{pmatrix} \sigma_x \\ \sigma_\theta \\ \tau_{x\theta} \end{pmatrix} = \begin{pmatrix} Q_{11} & Q_{12} & 0 \\ Q_{12} & Q_{22} & 0 \\ 0 & 0 & Q_{66} \end{pmatrix} \left(\begin{pmatrix} \varepsilon_x \\ \varepsilon_\theta \\ \gamma_{x\theta} \end{pmatrix} - \begin{pmatrix} 1 \\ 1 \\ 0 \end{pmatrix} \alpha_{\mathrm{T}}(z, T) \Delta T \right), \tag{22}$$

where σ_x, σ_θ, and $\tau_{x\theta}$ are the stress components. ε_x, ε_θ, and $\gamma_{x\theta}$ are the strain components. Q_{ij} $(i, j = 1, 2, 6)$ are the reduced stiffnesses. $\Delta T = T - T_{\mathrm{F}}$, where T_{F} is the temperature of the stress-free state, and is set as $T_{\mathrm{F}} = 300\,\mathrm{K}$.

For isotropic materials, Q_{11}, Q_{12}, Q_{22}, and Q_{66} are given by

$$\begin{cases} Q_{11} = Q_{22} = \dfrac{E(z,T)}{1-\mu(z,T)^2}, \\ Q_{12} = \dfrac{\mu(z,T)E(z,T)}{1-\mu(z,T)^2}, \\ Q_{66} = \dfrac{E(z,T)}{2(1+\mu(z,T))}. \end{cases} \tag{23}$$

Based on Love's shell theory, the strain relations are written as follows:

$$\varepsilon_x = \varepsilon_x^0 + z\chi_x, \quad \varepsilon_\theta = \varepsilon_\theta^0 + z\chi_\theta, \quad \gamma_{x\theta} = \gamma_{x\theta}^0 + 2z\chi_{x\theta}, \tag{24}$$

where χ_x, χ_θ, and $\chi_{x\theta}$ are the curvature variables and the twist variable of the middle plane. ε_x^0, ε_θ^0, and $\gamma_{x\theta}^0$ are the strains of the middle plane.

In Eq. (24), the corresponding variables are given by

$$\left(\varepsilon_x^0, \varepsilon_\theta^0, \gamma_{x\theta}^0\right) = \left(\frac{\partial u}{\partial x}, \frac{1}{R}\left(\frac{\partial v}{\partial \theta} + w\right), \frac{\partial v}{\partial x} + \frac{1}{R}\frac{\partial u}{\partial \theta}\right), \tag{25}$$

$$\left(\chi_x, \chi_\theta, \chi_{x\theta}\right) = \left(-\frac{\partial^2 w}{\partial x^2}, -\frac{1}{R^2}\left(\frac{\partial^2 w}{\partial \theta^2} - \frac{\partial v}{\partial \theta}\right), -\frac{1}{R}\left(\frac{\partial^2 w}{\partial x \partial \theta} - \frac{\partial v}{\partial x}\right)\right). \tag{26}$$

The internal forces and moments of an FGM shell are stated as follows:

$$\begin{pmatrix} N_x \\ N_\theta \\ N_{x\theta} \end{pmatrix} = \int_{-\frac{h}{2}}^{\frac{h}{2}} \begin{pmatrix} Q_{11} & Q_{12} & 0 \\ Q_{12} & Q_{22} & 0 \\ 0 & 0 & Q_{66} \end{pmatrix} \left(\begin{pmatrix} \varepsilon_x \\ \varepsilon_\theta \\ \gamma_{x\theta} \end{pmatrix} - \begin{pmatrix} \alpha_{\mathrm{T}}(z,T)\Delta T \\ \alpha_{\mathrm{T}}(z,T)\Delta T \\ 0 \end{pmatrix} \right) \mathrm{d}z, \tag{27}$$

$$\begin{pmatrix} M_x \\ M_\theta \\ M_{x\theta} \end{pmatrix} = \int_{-\frac{h}{2}}^{\frac{h}{2}} \begin{pmatrix} Q_{11} & Q_{12} & 0 \\ Q_{12} & Q_{22} & 0 \\ 0 & 0 & Q_{66} \end{pmatrix} \left(\begin{pmatrix} \varepsilon_x \\ \varepsilon_\theta \\ \gamma_{x\theta} \end{pmatrix} - \begin{pmatrix} \alpha_{\mathrm{T}}(z,T)\Delta T \\ \alpha_{\mathrm{T}}(z,T)\Delta T \\ 0 \end{pmatrix} \right) z\mathrm{d}z. \tag{28}$$

Introducing Eqs. (22) and (24) into Eqs. (27) and (28) gives the following constitutive equation:

$$\boldsymbol{N} = \boldsymbol{S}\boldsymbol{\varepsilon} - \boldsymbol{N}_{\mathrm{th}}, \tag{29}$$

where $\boldsymbol{N}$, $\boldsymbol{N}_{\mathrm{th}}$, and $\boldsymbol{\varepsilon}$ are defined as follows:

$$\begin{cases} \boldsymbol{N}^{\mathrm{T}} = \left(N_x, N_\theta, N_{x\theta}, M_x, M_\theta, M_{x\theta}\right), \\ \boldsymbol{\varepsilon}^{\mathrm{T}} = \left(\varepsilon_x^0, \varepsilon_\theta^0, \gamma_{x\theta}^0, \chi_x, \chi_\theta, 2\chi_{x\theta}\right), \\ \boldsymbol{N}_{\mathrm{th}}^{\mathrm{T}} = \left(N_x^{\mathrm{T}}, N_\theta^{\mathrm{T}}, N_{x\theta}^{\mathrm{T}}, M_x^{\mathrm{T}}, M_\theta^{\mathrm{T}}, M_{x\theta}^{\mathrm{T}}\right), \\ \begin{pmatrix} N_x^{\mathrm{T}} \\ N_\theta^{\mathrm{T}} \\ N_{x\theta}^{\mathrm{T}} \end{pmatrix} = \int_{-\frac{h}{2}}^{\frac{h}{2}} \begin{pmatrix} Q_{11} & Q_{12} & 0 \\ Q_{12} & Q_{22} & 0 \\ 0 & 0 & Q_{66} \end{pmatrix} \begin{pmatrix} \alpha_{\mathrm{T}}(z,T)\Delta T \\ \alpha_{\mathrm{T}}(z,T)\Delta T \\ 0 \end{pmatrix} \mathrm{d}z, \\ \begin{pmatrix} M_x^{\mathrm{T}} \\ M_\theta^{\mathrm{T}} \\ M_{x\theta}^{\mathrm{T}} \end{pmatrix} = \int_{-\frac{h}{2}}^{\frac{h}{2}} \begin{pmatrix} Q_{11} & Q_{12} & 0 \\ Q_{12} & Q_{22} & 0 \\ 0 & 0 & Q_{66} \end{pmatrix} \begin{pmatrix} \alpha_{\mathrm{T}}(z,T)\Delta T \\ \alpha_{\mathrm{T}}(z,T)\Delta T \\ 0 \end{pmatrix} z\mathrm{d}z, \end{cases} \tag{30}$$

and $\boldsymbol{S}$ is given by

$$\boldsymbol{S}=\begin{pmatrix} A_{11} & A_{12} & 0 & B_{11} & B_{12} & 0 \\ A_{12} & A_{22} & 0 & B_{12} & B_{22} & 0 \\ 0 & 0 & A_{66} & 0 & 0 & B_{66} \\ B_{11} & B_{12} & 0 & D_{11} & D_{12} & 0 \\ B_{12} & B_{22} & 0 & D_{12} & D_{22} & 0 \\ 0 & 0 & B_{66} & 0 & 0 & D_{66} \end{pmatrix}, \tag{31}$$

where A_{ij}, B_{ij}, and D_{ij} are the stretching, coupling, and bending stiffness coefficients given by

$$A_{ij}=\int_{-\frac{h}{2}}^{\frac{h}{2}} Q_{ij}\mathrm{d}z, \quad B_{ij}=\int_{-\frac{h}{2}}^{\frac{h}{2}} Q_{ij}z\mathrm{d}z, \quad D_{ij}=\int_{-\frac{h}{2}}^{\frac{h}{2}} Q_{ij}z^2\mathrm{d}z. \tag{32}$$

The strain energy and kinetic energy are expressed as follows:

$$U=\frac{1}{2}\int_0^L\int_0^{2\pi}(\boldsymbol{\varepsilon}^{\mathrm{T}}\boldsymbol{S}\boldsymbol{\varepsilon}-\boldsymbol{\varepsilon}^{\mathrm{T}}\boldsymbol{N}_{\mathrm{th}})R\mathrm{d}\theta\mathrm{d}x, \tag{33}$$

$$T_{\mathrm{k}}=\frac{1}{2}\int_0^L\int_0^{2\pi}\rho_{\mathrm{m}}\Big(\Big(\frac{\partial u}{\partial t}\Big)^2+\Big(\frac{\partial v}{\partial t}\Big)^2+\Big(\frac{\partial w}{\partial t}\Big)^2\Big)R\mathrm{d}\theta\mathrm{d}z, \tag{34}$$

where

$$\rho_{\mathrm{m}}=\int_{-\frac{h}{2}}^{\frac{h}{2}}\rho\left(z,T\right)\mathrm{d}z. \tag{35}$$

The FGM shell is considered to be simply supported at both ends. Therefore, we have

$$v=w=N_x=M_x=0 \quad \text{at} \quad x=0 \quad \text{and} \quad x=L. \tag{36}$$

The displacement functions satisfying the above boundary conditions can be expressed as follows:

$$\begin{cases} u=A\cos\left(m\pi x/L\right)\cos\left(n\theta\right)\cos\left(\omega t\right), \\ v=B\sin\left(m\pi x/L\right)\sin\left(n\theta\right)\cos\left(\omega t\right), \\ w=C\sin\left(m\pi x/L\right)\cos\left(n\theta\right)\cos\left(\omega t\right), \end{cases} \tag{37}$$

where A, B, and C are the constants representing the vibration amplitudes. m is the axial half-wave number, and n is the circumferential wave number, and ω is the natural circular frequency.

Thereafter, we use the Rayleigh-Ritz method to determine the natural frequencies of the porous FGM shell. To this end, we define the energy function Π via the Lagrangian function

$$\Pi=T_{\mathrm{kmax}}-U_{\mathrm{max}}, \tag{38}$$

where T_{kmax} and U_{max} are the maximum kinetic energy and the maximum strain energy, respectively.

The energy function is minimized by

$$\frac{\partial\Pi}{\partial A}=\frac{\partial\Pi}{\partial B}=\frac{\partial\Pi}{\partial C}=0. \tag{39}$$

From the above equation, we can obtain the following set of algebraic equations:

$$\begin{pmatrix} C_{11} & C_{12} & C_{13} \\ C_{21} & C_{22} & C_{23} \\ C_{31} & C_{32} & C_{33} \end{pmatrix} \begin{pmatrix} A \\ B \\ C \end{pmatrix} = \begin{pmatrix} 0 \\ 0 \\ 0 \end{pmatrix}, \tag{40}$$

where C_{ij} $(i, j = 1, 2, 3)$ denote the certain coefficients given in Appendix A.

In order to find the non-zero solutions, the determinant of the coefficient matrix must be equal to zero. Thus, the following polynomial equation is obtained:

$$a_1\omega^6 + a_2\omega^4 + a_3\omega^2 + a_4 = 0, \tag{41}$$

where a_i $(i = 1, 2, 3, 4)$ are constants. We can obtain three natural frequencies by solving Eq. (41). Among them, the smallest one is what we are interested in.

5 Results and discussion

In order to verify the correctness of the derivation in this paper, the simply supported homogeneous circular cylindrical shells are first considered. Two test cases are carried out, and the system parameters are as follows:

Case A (aluminium alloy): $L = 0.2\,\mathrm{m}$, $R = 0.1\,\mathrm{m}$, $h = 0.247 \times 10^{-3}\,\mathrm{m}$, $\rho = 2\,796\,\mathrm{kg{\cdot}m^{-3}}$, $\mu = 0.31$, $E = 71.02 \times 10^9\,\mathrm{Pa}$.

Case B (steel): $L = 0.2\,\mathrm{m}$, $R = 0.2\,\mathrm{m}$, $h = R/20$, $\rho = 7\,850\,\mathrm{kg{\cdot}m^{-3}}$, $\mu = 0.3$, $E = 210 \times 10^9\,\mathrm{Pa}$.

The natural frequencies obtained from the present method are compared with those obtained by Pellicano[37] (see Table 1). It is seen that the difference between the present results and published ones is less than 0.01%.

Table 1 Comparison of the natural frequencies for a homogeneous cylindrical shell at room temperature

Case	Mode		Natural frequency/Hz		
	m	n	Pellicano[37]	Present	Difference/%
A	1	7	484.60	484.545	0.010 00
	1	8	489.60	489.552	0.001 60
	1	9	546.20	546.196	0.000 70
	1	6	553.30	553.329	0.000 18
	1	10	636.80	636.807	0.001 00
	1	5	722.10	722.127	0.003 70
	1	11	750.70	750.664	0.000 80
	1	12	882.20	882.228	0.003 00
	2	10	968.10	968.088	0.000 20
	2	11	983.40	983.338	0.000 20
B	1	0	4 140.77	4 140.770	0.000 00
	2	0	4 788.66	4 788.660	0.000 00
	3	0	6 891.43	6 891.430	0.000 00
	4	0	10 657.70	10 657.700	0.000 00
	5	0	15 904.70	15 904.700	0.000 00

To further validate the present analysis, a simply supported perfect FGM cylindrical shell is taken into account to make a comparison with Loy et al.[9]. The FGM shell is assumed to be at room temperature, and the parameters are as follows:

Stainless steel: $E_{\mathrm{SS}} = 207.788 \times 10^9\,\mathrm{Pa}$, $\mu_{\mathrm{SS}} = 0.317\,756$, $\rho_{\mathrm{SS}} = 8\,166\,\mathrm{kg/m^3}$.

Nickel: $E_{\mathrm{Ni}} = 205.098 \times 10^9\,\mathrm{Pa}$, $\mu_{\mathrm{Ni}} = 0.31$, $\rho_{\mathrm{Ni}} = 8\,900\,\mathrm{kg/m^3}$.

The present results are compared with those in Ref. [9] (see Table 2), and they show very good agreement, which bespeaks the validity of the present analysis.

Table 2 Comparison of the natural frequencies for an FGM cylindrical shell at room temperature, where $m = 1$, $R = 1\,\mathrm{m}$, $h = 0.002\,\mathrm{m}$, and $L = 20\,\mathrm{m}$

n	$N = 0$		$N = 1$	
	Loy et al.[9]	Present	Loy et al.[9]	Present
1	13.548 0	13.548 00	13.211 0	13.211 00
2	4.592 0	4.591 39	4.480 0	4.479 00
3	4.263 3	4.262 49	4.156 9	4.156 20
4	7.225 0	7.224 50	7.038 4	7.037 90
5	11.542 0	11.541 70	11.241 0	11.240 70
6	16.897 0	16.897 00	16.455 0	16.454 80
7	23.244 0	23.244 00	22.635 0	22.634 90
8	30.573 0	30.573 00	29.771 0	29.771 30
9	38.881 0	38.881 40	37.862 0	37.861 50
10	48.168 0	48.168 30	46.905 0	46.904 60

In what follows, the FGM cylindrical shell with porosities shown in Fig. 1 will be treated. The properties of the constituent materials are listed in Table 3.

Table 3 Properties of materials[38]

		P_0	P_{-1}	P_1	P_2	P_3
Nickel	E/Pa	205.098×10^9	0	-2.794×10^{-4}	-3.998×10^{-9}	0
	μ	0.31	0	0	0	0
	$\rho/(\mathrm{kg\cdot m^{-3}})$	8 900	0	0	0	0
	$\kappa/(\mathrm{W\cdot(mK)^{-1}})$	187.66	0	-2.869×10^{-3}	4.005×10^{-6}	-1.983×10^{-9}
	$\alpha_\mathrm{T}/\mathrm{K^{-1}}$	$9.920\,9\times10^{-6}$	0	8.705×10^{-4}	0	0
Al_2O_3	E/Pa	349.55×10^9	0	-3.853×10^{-4}	-4.027×10^{-7}	-1.673×10^{-10}
	μ	0.26	0	0	0	0
	$\rho/(\mathrm{kg\cdot m^{-3}})$	3 950	0	0	0	0
	$\kappa/(\mathrm{W\cdot(mK)^{-1}})$	−14.087	−1 123.6	-6.227×10^{-3}	0	0
	$\alpha_\mathrm{T}/\mathrm{K^{-1}}$	$6.826\,9\times10^{-6}$	0	1.838×10^{-4}	0	0

Figures 3 and 4 show the variations of the elastic modulus E with the position z for three thermal load types. It can be seen that when no thermal load (UTR, $\Delta T_0 = 0\,\mathrm{K}$) is applied, the elastic modulus curve will be above the others and thus become the largest. Given the temperature change of 300 K, the UTR has the lowest elastic modulus among the three thermal load types. In addition, the NLTR has the larger elastic modulus than the LTR, but their difference is not very obvious. Especially, the difference becomes more and more inconsiderable with the increase in the power-law index N (see Figs. 3 and 4).

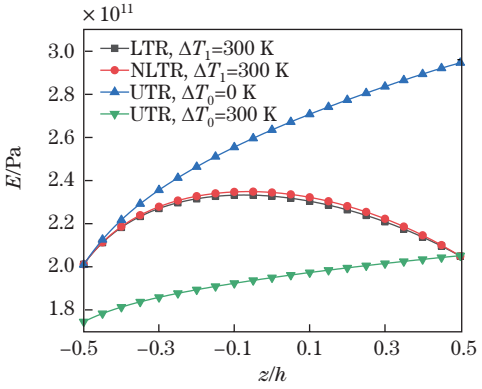

Fig. 3 Variations of the elastic modulus E with the position z, where $N = 0.5$, $\alpha = 0$, $T_0 = T_\mathrm{M} = 300\,\mathrm{K}$, $R = 1\,\mathrm{m}$, $h = 0.002\,\mathrm{m}$, and $L = 20\,\mathrm{m}$ (color online)

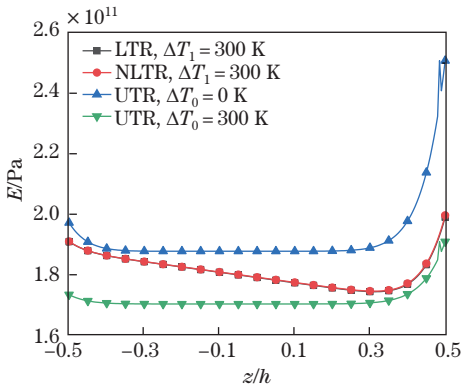

Fig. 4 Variations of the elastic modulus E with the position z, where $N = 20$, $\alpha = 0$, $T_0 = T_{\mathrm{M}} = 300\,\mathrm{K}$, $R = 1\,\mathrm{m}$, $h = 0.002\,\mathrm{m}$, and $L = 20\,\mathrm{m}$ (color online)

Table 4 shows the variations of the natural frequencies of a perfect FGM shell against the power-lower index N for different thermal load types. It is clear that the natural frequencies under the UTR are the smallest among the three thermal load types. Additionally, the natural frequencies under the LTR and those under the NLTR have little differences. This indicates that the LTR can give good accuracy instead of the NLTR for perfect thin FGM shells. Furthermore, one can find that the fundamental natural frequency corresponds to the mode $(m = 1, n = 3)$.

Table 4 Variations of the natural frequencies (rad·s^{-1}) against N for different thermal load types, where $\alpha = 0$, $T_0 = T_{\mathrm{M}} = 300\,\mathrm{K}$, $\Delta T_i = 300\,\mathrm{K}$ $(i = 0, 1)$, $R = 1\,\mathrm{m}$, $h = 0.002\,\mathrm{m}$, and $L = 20\,\mathrm{m}$

m	n	$N = 0$			$N = 1$			$N = 30$		
		UTR	LTR	NLTR	UTR	LTR	NLTR	UTR	LTR	NLTR
1	1	121.78	135.26	135.26	91.31	96.60	96.87	73.94	75.82	75.84
1	2	41.19	45.72	45.72	30.78	32.53	32.62	25.05	25.69	25.69
1	3	37.76	41.70	41.70	28.27	29.63	29.70	23.22	23.81	23.81
1	4	63.76	70.29	70.29	47.98	50.17	50.26	39.34	40.34	40.34
1	5	101.81	112.22	112.22	76.74	80.21	80.36	62.84	64.44	64.45
2	1	447.46	496.99	496.99	335.31	354.71	355.70	271.35	278.25	278.31
2	2	155.26	172.44	172.44	116.31	123.03	123.38	94.31	96.71	96.73
2	3	81.19	90.07	90.07	60.61	64.00	64.17	49.45	50.71	50.72
2	4	76.31	84.31	84.31	57.07	59.88	60.00	46.86	48.06	48.07
2	5	105.59	116.45	116.45	79.34	82.99	83.15	65.10	66.76	66.77
3	1	899.35	998.90	998.90	673.52	712.47	714.47	544.67	558.53	558.65
3	2	337.31	374.66	374.66	252.80	267.43	268.18	204.83	210.05	210.09
3	3	167.85	186.38	186.38	125.54	132.75	133.12	102.02	104.62	104.64
3	4	114.91	127.34	127.34	85.74	90.38	90.61	70.15	71.93	71.95
3	5	119.80	132.32	132.32	89.64	94.00	94.20	73.63	75.50	75.51

Table 5 shows the variations of the fundamental frequency of a perfect FGM shell for different types of thermal load. Again, it is found that the LTR and NLTR result in almost the same fundamental frequencies, independent of the temperature change. Moreover, the fundamental frequency shows a decreasing tendency when the temperature change increases.

Table 6 lists the fundamental natural frequencies of an FGM shell with porosities for different α and N. It shows that when the power-law index is relatively small, e.g., $N = 0.5$, the frequency increases with the rise of the porosity volume fraction. However, when the power-law index is large, e.g., $N = 20$, the natural frequency decreases with the rise of the porosity volume fraction. The above phenomenon shows that the porosity effect is affected by the power-law

index. Furthermore, Porosity-II FGM shell can lead to larger natural frequencies than its counterpart Porosity-I except for $N = 0$.

Table 5 Variations of the fundamental natural frequency (rad·s^{-1}) against ΔT_i ($i = 0, 1$) for different thermal load types and N, where $\alpha = 0$, $m = 1$, $n = 3$, $T_0 = T_{\mathrm{M}} = 300\,\mathrm{K}$, $R = 1\,\mathrm{m}$, $h = 0.002\,\mathrm{m}$, and $L = 20\,\mathrm{m}$

ΔT_i ($i = 0, 1$)	Thermal load	$N = 0.5$	$N = 1$	$N = 5$
$\Delta T_0 = \Delta T_1 = 100\,\mathrm{K}$	UTR	34.05	30.87	26.35
	LTR	34.60	31.25	26.59
	NLTR	34.62	31.27	26.60
$\Delta T_0 = \Delta T_1 = 200\,\mathrm{K}$	UTR	32.54	29.68	25.61
	LTR	33.74	30.52	26.09
	NLTR	33.78	30.56	26.11
$\Delta T_0 = \Delta T_1 = 300\,\mathrm{K}$	UTR	30.71	28.27	24.75
	LTR	32.70	29.63	25.50
	NLTR	32.76	29.70	25.53

Table 6 Variations of the fundamental natural frequency (rad·s^{-1}) against the power-law index N for different α, where $m = 1$, $n = 3$, $T_0 = T_{\mathrm{M}} = 300\,\mathrm{K}$, $\Delta T_i = 300\,\mathrm{K}$ ($i = 0, 1$), $R = 1\,\mathrm{m}$, $h = 0.002\,\mathrm{m}$, and $L = 20\,\mathrm{m}$

N	Thermal load	Perfect ($\alpha = 0.0$)	Porosity-I		Porosity-II	
			$\alpha = 0.1$	$\alpha = 0.2$	$\alpha = 0.1$	$\alpha = 0.2$
0.0 (Al_2O_3)	UTR	37.76	39.12	41.12	38.78	39.97
	LTR	41.70	43.33	45.73	42.84	44.18
	NLTR	41.70	43.33	45.73	42.84	44.18
0.5	UTR	30.71	30.82	31.03	31.10	31.55
	LTR	32.70	32.80	33.01	33.11	33.57
	NLTR	32.76	32.87	33.07	33.17	33.63
3.0	UTR	25.52	25.08	24.60	25.61	25.71
	LTR	26.38	25.80	25.15	26.43	26.50
	NLTR	26.42	25.84	25.19	26.47	26.54
20.0	UTR	23.55	22.94	22.27	23.55	23.55
	LTR	24.20	23.45	22.61	24.16	24.12
	NLTR	24.21	23.46	22.62	24.17	24.13
$+\infty$ (nickel)	UTR	23.19	22.55	21.84	23.17	23.15
	LTR	23.76	22.98	22.09	23.70	23.65
	NLTR	23.76	22.98	22.09	23.70	23.65

Table 7 shows the fundamental natural frequencies of Porosity-I FGM shells for various thickness-to-radius ratios. A very obvious tendency can be found that the frequency increases as the thickness-to-radius ratio increases. In Table 8, the fundamental natural frequencies of Porosity-II FGM shells for various length-to-radius ratios are tabulated. With the increase in the length-to-radius ratio, the fundamental frequencies decrease. Moreover, one may find that the frequency changes insignificantly after the length-to-radius ratio exceeds 30. This can be understood because the frequencies of a cylindrical shell get close to those of its beam counterpart when the length-to-radius ratio is large enough. In this case, a shell model can be simplified to a beam model without considering the hollow.

In Table 9, the reduction of the first three order natural frequencies are tabulated for Porosity-I FGM shells under the NLTR. Compared with the FGM shell without thermal load ($\Delta T_1 = 0$), the natural frequencies of the FGM shell with thermal load ($\Delta T_1 = 300\,\mathrm{K}$) decrease by about 7%.

Table 7 Variations of the fundamental natural frequency (rad·s^{-1}) against the thickness-to-radius ratio (Porosity-I, $N = 3$, $m = 1$, $n = 3$, $T_0 = T_{\mathrm{M}} = 300\,\mathrm{K}$, $\Delta T_i = 300\,\mathrm{K}$ ($i = 0, 1$), $R = 1\,\mathrm{m}$, and $L = 20\,\mathrm{m}$)

α	Thermal load	h/R					
		0.002	0.006	0.01	0.014	0.018	0.022
0.0	UTR	25.52	68.20	112.53	157.12	201.78	246.48
	LTR	26.38	70.44	116.23	162.28	208.42	254.59
	NLTR	26.42	70.55	116.40	162.52	208.73	254.97
0.1	UTR	25.08	66.90	110.38	154.10	197.90	241.73
	LTR	25.80	68.78	113.46	158.41	203.43	248.49
	NLTR	25.84	68.88	113.63	158.64	203.73	248.86
0.2	UTR	24.60	65.53	108.09	150.90	193.79	236.70
	LTR	25.15	66.95	110.42	154.15	197.96	241.79
	NLTR	25.19	67.05	110.58	154.38	198.25	242.14

Table 8 Variations of the fundamental natural frequency (rad·s^{-1}) against the length-to-radius ratio (Porosity-II, $N = 3$, $m = 1$, $n = 3$, $T_0 = T_{\mathrm{M}} = 300\,\mathrm{K}$, $\Delta T_i = 300\,\mathrm{K}$ ($i = 0, 1$), $R = 1\,\mathrm{m}$, and $h = 0.002\,\mathrm{m}$)

α	Thermal load	h/R					
		10	20	30	40	50	60
0.0	UTR	54.32	25.52	22.98	22.54	22.42	22.38
	LTR	56.24	26.38	23.74	23.28	23.15	23.11
	NLTR	56.34	26.42	23.78	23.31	23.19	23.15
0.1	UTR	53.63	25.08	22.55	22.11	21.99	21.95
	LTR	55.27	25.80	23.19	22.73	22.60	22.56
	NLTR	55.37	25.84	23.22	22.76	22.64	22.60
0.2	UTR	52.81	24.60	22.09	21.65	21.54	21.49
	LTR	54.13	25.15	22.57	22.12	22.00	21.96
	NLTR	54.22	25.19	22.61	22.15	22.03	21.99

Table 9 Reduction of the first three order natural frequencies (rad·s^{-1}) under NLTR (Porosity-I, $N = 0.5$, $T_{\mathrm{M}} = 300\,\mathrm{K}$, $R = 1\,\mathrm{m}$, $h = 0.002\,\mathrm{m}$, and $L = 20\,\mathrm{m}$)

α	$m = 1$, $n = 3$			$m = 1$, $n = 2$			$m = 1$, $n = 4$		
	ΔT_1/K		Reduction	ΔT_1/K		Reduction	ΔT_1/K		Reduction
	0	300		0	300		0	300	
0.0	35.32	32.76	7.25%	38.76	36.10	6.86%	59.73	55.34	7.35%
0.1	35.49	32.87	7.38%	39.21	36.46	7.01%	59.89	55.39	7.51%
0.2	35.79	33.07	7.60%	39.79	36.91	7.24%	60.26	55.61	7.72%

Figure 5 presents the effects of the porosity volume fraction on the fundamental frequencies of Porosity-I and Porosity-II FGM shells. It is clear that the fundamental frequencies decrease with the increasing power-law index. For the Porosity-I FGM shell, larger porosity volume fraction leads to higher frequency when N is small. When N increases, this trend reverses completely, i.e., larger porosity volume fraction leads to lower frequency. For the Porosity-II FGM shell, it is also found that larger porosity volume fraction leads to higher frequency when $N < 1$, while the porosity effect is not obvious when $N > 1$.

To compare the difference of the two types of porosity distribution, Fig. 6 shows the comparison of the first two natural frequencies for Porosity-I and Porosity-II FGM cylindrical

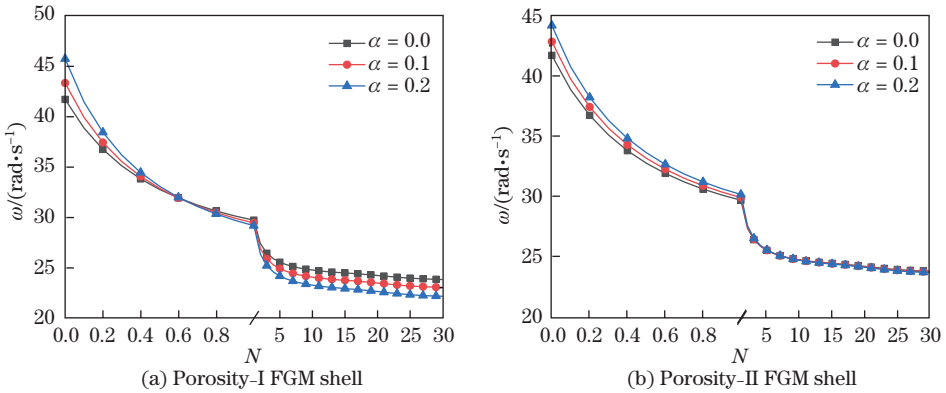

(a) Porosity-I FGM shell (b) Porosity-II FGM shell

Fig. 5 Variations of the fundamental natural frequency against the power-law index N for different porosity volume fractions under the NLTR, where $m = 1$, $n = 3$, $T_{\mathrm{M}} = 300\,\mathrm{K}$, $\Delta T_i = 300\,\mathrm{K}$ $(i = 0,\ 1)$, $R = 1\,\mathrm{m}$, $h = 0.002\,\mathrm{m}$, and $L = 20\,\mathrm{m}$ (color online)

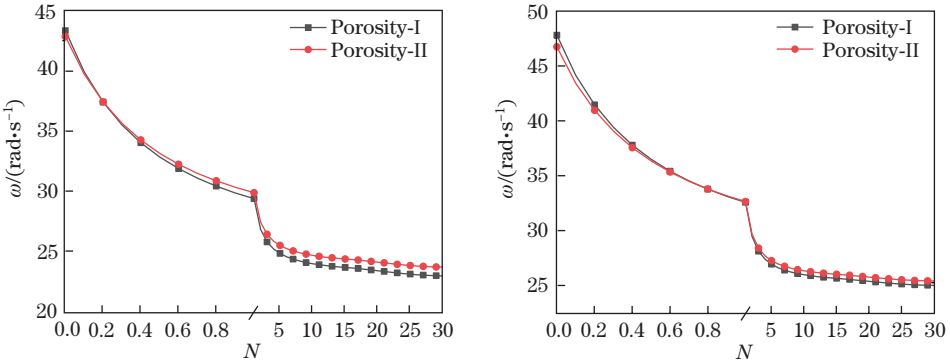

(a) Fundamental natural frequency ($m = 1$, $n = 3$) (b) Second natural frequency ($m = 1$, $n = 2$)

Fig. 6 Comparison of the first two order natural frequencies for Porosity-I and Porosity-II FGM shells under the NLTR, where $\alpha = 0.1$, $T_{\mathrm{M}} = 300\,\mathrm{K}$, $\Delta T_i = 300\,\mathrm{K}$ $(i = 0,\ 1)$, $R = 1\,\mathrm{m}$, $h = 0.002\,\mathrm{m}$, and $L = 20\,\mathrm{m}$ (color online)

shells. It is found that the effect of porosity distribution depends on the power-law index. When the power-law index is small, the Porosity-I results in higher natural frequencies. With the increase in the power-law index, the natural frequencies of the Porosity-II FGM shell gradually exceed those of the Porosity-I FGM shell. Therefore, the Porosity-II FGM shell has higher natural frequencies than the Porosity-I one at large power-law indices.

Figure 7 shows the variations of the fundamental natural frequencies against the temperature change for perfect Porosity-I and Porosity-II cylindrical FGM shells. It can be seen that all the fundamental frequencies of the three shells decrease with the increasing temperature change. In addition, the Porosity-I FGM shell has the lowest fundamental frequency, while the perfect one has the highest frequency.

In order to further confirm the above conclusions, another FGM cylindrical shell composed of zirconia-stainless steel is considered. Their material properties are listed in Table 10. The natural frequencies of the zirconia-stainless steel FGM cylindrical shell are given for various parameters (see Tables 11 and 12). From Tables 11 and 12, we can see that an FGM cylindrical shell made of different component materials also gives similar qualitative results as before, which confirms our viewpoint again.

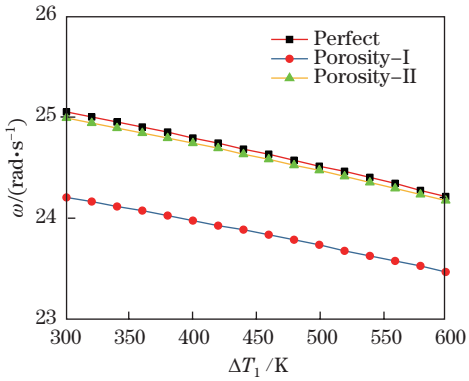

Fig. 7 Variations of the fundamental natural frequency against the temperature change for different types of porosity distribution under the NLTR, where $m = 1$, $n = 3$, $\alpha = 0.1$, $N = 20$, $T_{\mathrm{M}} = 300\,\mathrm{K}$, $\Delta T_i = 300\,\mathrm{K}$ $(i = 0, 1)$, $R = 1\,\mathrm{m}$, $h = 0.002\,\mathrm{m}$, and $L = 20\,\mathrm{m}$ (color online)

Table 10 Properties of materials[38]

Material	Parameter	P_0	P_{-1}	P_1	P_2	P_3
Zirconia	E/Pa	244.27×10^{9}	0	-1.371×10^{-3}	1.214×10^{-6}	-3.681×10^{-10}
	μ	0.288 2	0	1.133×10^{-4}	0	0
	ρ/(kg·m^{-3})	5 700	0	0	0	0
	κ/(W·(mK)$^{-1}$)	1.700	0	1.276×10^{-4}	6.648×10^{-8}	0
	α_{T}/K^{-1}	12.766×10^{-6}	0	-1.491×10^{-3}	1.006×10^{-5}	-6.778×10^{-11}
Stainless steel	E/Pa	201.04×10^{9}	0	3.079×10^{-4}	-6.534×10^{-7}	0
	μ	0.326 2	0	-2.002×10^{-4}	3.797×10^{-7}	0
	ρ/(kg·m^{-3})	8 166	0	0	0	0
	κ/(W·(mK)$^{-1}$)	15.379	0	-1.264×10^{-3}	2.092×10^{-6}	-7.223×10^{-10}
	α_{T}/K^{-1}	12.330×10^{-6}	0	8.086×10^{-4}	0	0

Table 11 Variations of the natural frequencies (rad·s^{-1}) against N for FGM shells composed of zirconia-stainless steel, where $\alpha = 0$, $T_0 = T_{\mathrm{M}} = 300\,\mathrm{K}$, $\Delta T_i = 300\,\mathrm{K}$ $(i = 0, 1)$, $R = 1\,\mathrm{m}$, $h = 0.002\,\mathrm{m}$, and $L = 20\,\mathrm{m}$

m	n	$N = 0$			$N = 1$			N=30		
		UTR	LTR	NLTR	UTR	LTR	NLTR	UTR	LTR	NLTR
1	1	80.81	85.63	85.63	81.26	84.13	84.86	81.58	83.78	83.89
1	2	27.37	29.03	29.03	27.47	28.46	28.70	27.66	28.43	28.46
1	3	25.35	26.89	26.89	25.39	26.15	26.31	25.75	26.39	26.42
1	4	42.94	45.50	45.50	43.07	44.23	44.47	43.68	44.67	44.73
1	5	68.60	72.66	72.66	68.85	70.65	71.04	69.80	71.33	71.43
2	1	296.55	314.31	314.31	298.12	308.72	311.41	299.20	307.36	307.76
2	2	103.06	109.24	109.24	103.60	107.29	108.21	104.07	106.91	107.04
2	3	54.03	57.32	57.32	54.18	56.11	56.55	54.63	56.14	56.21
2	4	51.18	54.28	54.28	51.24	52.83	53.16	51.95	53.26	53.33
2	5	71.08	75.33	75.33	71.25	73.22	73.63	72.28	73.95	74.05

Table 12 Natural frequencies (rad·s^{-1}) of the FGM shell composed of zirconia-stainless steel, where $\alpha = 0.2$, $N = 3$, $T_0 = T_{\rm M} = 300\,{\rm K}$, $\Delta T_i = 300\,{\rm K}$ $(i = 0,\ 1)$, $R = 1\,{\rm m}$, $h = 0.002\,{\rm m}$, and $L = 20\,{\rm m}$

m	n	Perfect			Porosity-I			Porosity-II		
		UTR	LTR	NLTR	UTR	LTR	NLTR	UTR	LTR	NLTR
1	1	81.43	83.84	84.33	81.53	83.74	84.18	81.49	83.81	84.26
1	2	27.51	28.34	28.50	27.47	28.23	28.37	27.55	28.35	28.49
1	3	25.18	25.85	25.97	24.70	25.30	25.42	25.50	26.16	26.28
1	4	42.57	43.59	43.79	41.52	42.42	42.62	43.30	44.30	44.51
1	5	68.03	69.60	69.93	66.29	67.70	68.02	69.23	70.79	71.13
2	1	298.70	307.62	309.41	299.54	307.74	309.35	299.16	307.75	309.42
2	2	103.82	106.92	107.53	103.89	106.73	107.28	103.87	106.85	107.42
2	3	54.19	55.83	56.13	54.00	55.49	55.76	54.33	55.91	56.19
2	4	50.88	52.26	52.51	50.00	51.24	51.48	51.46	52.81	53.06
2	5	70.48	72.20	72.54	68.80	70.34	70.67	71.62	73.32	73.66

6 Conclusions

In this study, the free vibrations of FGM cylindrical shells with porosities are examined under various temperature conditions. The present mathematical model is based on Love's shell theory. The Rayleigh-Ritz method is utilized to determine the natural frequencies of the porous FGM cylindrical shells. The results show that the porosities can affect the vibration characteristics of the FGM cylindrical shells. However, this effect will be affected by the power-law index. When the porosity volume fraction increases, the natural frequencies of the FGM cylindrical shells decrease or increase, depending on the value of the power-law index. Additionally, the natural frequencies increase with the increase in the thickness-to-radius ratio, and decrease with the increases in the temperature change and the length-to-radius ratio of the porous FGM shells.

Among various types of thermal loads, i.e., the UTR, the LTR, and the NLTR, the UTR always corresponds to the lowest frequency. The frequency differences between the UTR and the other two types of loads are quite obvious. Moreover, the natural frequencies obtained from the LTR are nearly the same as those from the NLTR, which means that the LTR model has high accuracy. In view of the complexity of the NLTR, this study demonstrates that the LTR can be reasonably used to replace the NLTR in the vibration analysis of thin FGM cylindrical shells, no matter with or without porosities.

References

[1] KOIZUMI, M. FGM activities in Japan. *Composites Part B*: *Engineering*, **28**, 1–4 (1997)

[2] WANG, Y. and ZU, J. W. Nonlinear oscillations of sigmoid functionally graded material plates moving in longitudinal direction. *Applied Mathematics and Mechanics* (*English Edition*), **38**(11), 1533–1550 (2017) https://doi.org/10.1007/s10483-017-2277-9

[3] WAN, Z. and LI, S. Thermal buckling analysis of functionally graded cylindrical shells. *Applied Mathematics and Mechanics* (*English Edition*), **38**(8), 1059–1070 (2017) https://doi.org/10.1007/s10483-017-2225-7

[4] WANG, Y. Q. and ZU, J. W. Nonlinear steady-state responses of longitudinally traveling functionally graded material plates in contact with liquid. *Composite Structures*, **164**, 130–144 (2017)

[5] DUNG, D. V., NGA, N. T., and HOA, L. K. Nonlinear stability of functionally graded material (FGM) sandwich cylindrical shells reinforced by FGM stiffeners in thermal environment. *Applied Mathematics and Mechanics* (*English Edition*), **38**(5), 647–670 (2017) https://doi.org/10.1007/s10483-017-2198-9

[6] ZHANG, W., YANG, J., and HAO, Y. Chaotic vibrations of an orthotropic FGM rectangular plate based on third-order shear deformation theory. *Nonlinear Dynamics*, **59**, 619–660 (2010)

[7] ZHANG, W., HAO, Y., GUO, X., and CHEN, L. Complicated nonlinear responses of a simply supported FGM rectangular plate under combined parametric and external excitations. *Meccanica*, **47**, 985–1014 (2012)

[8] WANG, Y. Q., HUANG, X. B., and LI, J. Hydroelastic dynamic analysis of axially moving plates in continuous hot-dip galvanizing process. *International Journal of Mechanical Sciences*, **110**, 201–216 (2016)

[9] LOY, C. T., LAM, K. Y., and REDDY, J. N. Vibration of functionally graded cylindrical shells. *International Journal of Mechanical Sciences*, **41**, 309–324 (1999)

[10] PATEL, B., GUPTA, S., LOKNATH, M., and KADU, C. Free vibration analysis of functionally graded elliptical cylindrical shells using higher-order theory. *Composite Structures*, **69**, 259–270 (2005)

[11] SHAH, A. G., MAHMOOD, T., and NAEEM, M. N. Vibrations of FGM thin cylindrical shells with exponential volume fraction law. *Applied Mathematics and Mechanics* (*English Edition*), **30**(5), 607–615 (2009) https://doi.org/10.1007/s10483-009-0507-x

[12] MATSUNAGA, H. Free vibration and stability of functionally graded circular cylindrical shells according to a 2D higher-order deformation theory. *Composite Structures*, **88**, 519–531 (2009)

[13] ARSHAD, S. H., NAEEM, M. N., SULTANA, N., SHAH, A. G., and IQBAL, Z. Vibration analysis of bi-layered FGM cylindrical shells. *Archive of Applied Mechanics*, **81**, 319–343 (2011)

[14] DING, H., TAN, X., and DOWELL, E. H. Natural frequencies of a super-critical transporting Timoshenko beam. *European Journal of Mechanics-A/Solids*, **66**, 79–93 (2017)

[15] TAN, X., MAO, X. Y., DING, H., and CHEN, L. Q. Vibration around non-trivial equilibrium of a supercritical Timoshenko pipe conveying fluid. *Journal of Sound and Vibration*, **428**, 104–118 (2018)

[16] CARRERA, E., BRISCHETTO, S., CINEFRA, M., and SOAVE, M. Effects of thickness stretching in functionally graded plates and shells. *Composites Part B*: *Engineering*, **42**, 123–133 (2011)

[17] BICH, D. H. and XUAN, N. N. Nonlinear vibration of functionally graded circular cylindrical shells based on improved Donnell equations. *Journal of Sound and Vibration*, **331**, 5488–5501 (2012)

[18] STROZZI, M. and PELLICANO, F. Nonlinear vibrations of functionally graded cylindrical shells. *Thin-Walled Structures*, **67**, 63–77 (2013)

[19] TORNABENE, F., FANTUZZI, N., and BACCIOCCHI, M. Free vibrations of free-form doubly-curved shells made of functionally graded materials using higher-order equivalent single layer theories. *Composites Part B*: *Engineering*, **67**, 490–509 (2014)

[20] BHANGALE, R. K., GANESAN, N., and PADMANABHAN, C. Linear thermoelastic buckling and free vibration behavior of functionally graded truncated conical shells. *Journal of Sound and Vibration*, **292**, 341–371 (2006)

[21] HADDADPOUR, H., MAHMOUDKHANI, S., and NAVAZI, H. Free vibration analysis of functionally graded cylindrical shells including thermal effects. *Thin-Walled structures*, **45**, 591–599 (2007)

[22] ZHAO, X., LEE, Y., and LIEW, K. M. Thermoelastic and vibration analysis of functionally graded cylindrical shells. *International Journal of Mechanical Sciences*, **51**, 694–707 (2009)

[23] KIANI, Y., SHAKERI, M., and ESLAMI, M. Thermoelastic free vibration and dynamic behaviour of an FGM doubly curved panel via the analytical hybrid Laplace-Fourier transformation. *Acta Mechanica*, **223**, 1199–1218 (2012)

[24] ZHANG, W., HAO, Y. X., and YANG, J. Nonlinear dynamics of FGM circular cylindrical shell with clamped-clamped edges. *Composite Structures*, **94**, 1075–1086 (2012)

[25] DU, C., LI, Y., and JIN, X. Nonlinear forced vibration of functionally graded cylindrical thin shells. *Thin-Walled Structures*, **78**, 26–36 (2014)

[26] LIU, Y. Z., HAO, Y. X., ZHANG, W., CHEN, J., and LI, S. B. Nonlinear dynamics of initially imperfect functionally graded circular cylindrical shell under complex loads. *Journal of Sound and Vibration*, **348**, 294–328 (2015)

[27] DUC, N. D. Nonlinear thermal dynamic analysis of eccentrically stiffened S-FGM circular cylindrical shells surrounded on elastic foundations using the Reddy's third-order shear deformation shell theory. *European Journal of Mechanics-A/Solids*, **58**, 10–30 (2016)

[28] SHENG, G. G. and WANG, X. The non-linear vibrations of rotating functionally graded cylindrical shells. *Nonlinear Dynamics*, **87**, 1095–1109 (2017)

[29] ZHU, J., LAI, Z., YIN, Z., JEON, J., and LEE, S. Fabrication of ZrO_2-NiCr functionally graded material by powder metallurgy. *Materials Chemistry and Physics*, **68**, 130–135 (2001)

[30] WATTANASAKULPONG, N. and CHAIKITTIRATANA, A. Flexural vibration of imperfect functionally graded beams based on Timoshenko beam theory: Chebyshev collocation method. *Meccanica*, **50**, 1331–1342 (2015)

[31] EBRAHIMI, F., GHASEMI, F., and SALARI, E. Investigating thermal effects on vibration behavior of temperature-dependent compositionally graded Euler beams with porosities. *Meccanica*, **51**, 223–249 (2016)

[32] WANG, Y. Q. and ZU, J. W. Vibration characteristics of moving sigmoid functionally graded plates containing porosities. *International Journal of Mechanics and Materials in Design* (2017) https://doi.org/10.1007/s10999-017-9385-2

[33] WANG, Y. Q. Electro-mechanical vibration analysis of functionally graded piezoelectric porous plates in the translation state. *Acta Astronautica*, **143**, 263–271 (2018)

[34] WANG, Y. Q. and ZU, J. W. Nonlinear dynamics of a translational FGM plate with strong mode interaction. *International Journal of Structural Stability and Dynamics*, **18**, 1850031 (2018)

[35] JAVAHERI, R. and ESLAMI, M. Thermal buckling of functionally graded plates. *AIAA Journal*, **40**, 162–169 (2002)

[36] AMABILI, M. *Nonlinear Vibrations and Stability of Shells and Plates*, Cambridge University Press, Cambridge (2008)

[37] PELLICANO, F. Vibrations of circular cylindrical shells: theory and experiments. *Journal of Sound and Vibration*, **303**, 154–170 (2007)

[38] REDDY, J. N. and CHIN, C. D. Thermomechanical analysis of functionally graded cylinders and plates. *Journal of Thermal Stresses*, **21**, 593–626 (1998)

Appendix A

The coefficients C_{ij} $(i, j = 1, 2, 3)$ in Eq. (40) are defined as follows:

$$C_{11} = \frac{A_{11}m^2\pi^3 R}{2L} + \frac{A_{66}\pi n^2 L}{2R} - \xi\omega^2,$$

$$C_{12} = -\frac{mn\pi^2}{2}\Big(A_{12} + A_{66} + \frac{B_{12}}{R} + \frac{2B_{66}}{R}\Big),$$

$$C_{13} = -\frac{m\pi^2}{2}\Big(A_{12} + \frac{B_{12}n^2}{R} + \frac{2B_{66}n^2}{R} + \frac{B_{11}m^2\pi^2 R}{L^2}\Big),$$

$$C_{22} = \frac{m^2\pi^3}{L}\Big(\frac{A_{66}R}{2} + 2B_{66} + \frac{2D_{66}}{R}\Big) + \frac{n^2 L\pi}{R}\Big(\frac{A_{22}}{2} + \frac{B_{22}}{R} + \frac{D_{22}}{2R^2}\Big) - \xi\omega^2,$$

$$C_{23} = \frac{m^2 n\pi^3}{L}\Big(\frac{B_{12}}{2} + B_{66} + \frac{D_{12}}{2R} + \frac{D_{66}}{R}\Big) + \frac{n\pi L}{2R}\Big(A_{22} + \frac{B_{22}}{R}\Big) + \frac{n^3\pi L}{2R^2}\Big(B_{22} + \frac{D_{22}}{R}\Big),$$

$$C_{33} = \frac{m^2n^2\pi^3}{LR}(D_{12} + 2D_{66}) + \frac{n^2\pi L}{R^2}\Big(B_{22} + \frac{D_{22}n^2}{2R}\Big) + \frac{m^2\pi^3}{L}\Big(B_{12} + \frac{D_{11}m^2\pi^2 R}{2L^2}\Big) + \frac{A_{22}\pi L}{2R} - \xi\omega^2,$$

$$\xi = \frac{\pi RL}{2}\rho_{\mathrm{m}}.$$